Hindawi
Advances in Materials Science and Engineering
Volume 2021, Article ID 6620577, 13 pages
https://doi.org/10.1155/2021/6620577

Research Article

Experimental Study on CFRP-Confined Circularized Concrete-Filled Square Steel Tube Short Columns

Yuchuan Wen, Zhongjun Hu, Anningjing Li, Quanheng Li, Xuepeng Li, and Yan Xu

College of Construction Engineering, Jilin University, Changchun 130026, China

Correspondence should be addressed to Zhongjun Hu; huzj@jlu.edu.cn

Received 17 November 2020; Revised 17 December 2020; Accepted 4 March 2021; Published 17 March 2021

Academic Editor: Peng Zhang

This study investigates the suitability of the circularization technique for strengthening square concrete-filled square steel tube (CFSST) short columns. A total of 16 specimens were tested under axial compression. The main parameters under investigation were concrete strength, the thickness of arc cement mortar layer components (CAM), and the layers of carbon fiber-reinforced polymer (CFRP) sheets. Test results indicated that the failure mode of CFRP-confined circularized CFSST (C-C-CFSST) columns was similar to that of CFRP-confined concrete columns. The CFRP-confined circularized strengthening method can increase confinement efficacy and reduce the stress concentration at the corners of CFSST columns. Three existing CFRP-confined concrete stress-strain models were evaluated using the test results. The predictions of the Lam and Teng stress-strain model agree well with the test data.

1. Introduction

Concrete-filled steel tube (CFST) has the advantages of high bearing capacity and ductility and is widely used in civil structures [1, 2]. However, the exposed CFST structures are easily failed by corrosion in engineering practice, especially in the moisture environment [3–5]. When the corrosion occurs on steel tube, the durability and bearing capacity of CFST will degrade [6]. Consequently, finding a method to enhance the corrosion resistance of CFST columns is necessary [7].

Fiber-reinforced polymer (FRP) composites have been widely used in retrofitting existing columns [8, 9]. FRP-confined concrete has been proven to be feasible in theoretical research and engineering practice [10]. Strengthening CFST columns with FRP material has the dual advantages of improving bearing capacity and durability [11–13].

In recent years, concrete-filled square steel tube (CFSST) has been increasingly applied in various building structures because of its advantages of easy joint connection and construction [14–16].

Tao, Han, and Wang studied the section shape influence on the axial compression performance of CFRP-confined CFST short columns. The results indicated that the CFRP confinement efficacy of a CFSST column is lower than a circular CFST column because of the stress concentration at the corners of the square steel tube and the reduction of the effective area of the confined section [17, 18].

To improve the confinement efficiency of CFSST columns by CFRP jackets and to reduce stress concentration, the circularizing technique has been proven to be an effective method before FRP wrapping by some scholars. The experimental study of Priestley and Seible first indicated that shape modification by bonding concrete segments can improve the confinement efficiency of CFRP jackets [19]. Hadi et al. carried out relevant research on the CFRP-confined arc-treated concrete rectangular columns; the results show that using precast concrete arc-treated components as transitions between CFRP and rectangular columns could significantly reduce stress concentration and enhance the effective constraint area of the cross section [20, 21]. The above studies showed that circularizing concrete columns by bonding precast segments can increase the axial load capacity and change the stress-strain curve from softening to hardening the branch of reinforced concrete (RC) columns [20].

Yang et al. performed an experimental study on the axial compressive performance of rectangular concrete-filled FRP-steel composite tube columns for various corner radiuses and proposed that FRP-confined CFSST concrete stress-strain curve can be divided into four phases (i.e., initial linear phase, transition to yield phase, hardening phase, and residual phase). Different corner radii significantly affect the confinement effectiveness and the third phase of the FRP-confined CFSST stress-strain curve [22]. Most of the existing CFSST columns have sharp corners, which cause stress concentration, and the CFSST columns cannot round the corners similar to RC columns in practical engineering. Therefore, shape modification before FRP wrapping may effectively reduce stress concentration. To solve this problem further, an experimental study was undertaken to investigate the suitability of the circularization technique for strengthening CFSST short columns. This study utilizes the bonding CAM components between FRP and the CFSST column as a circularizing method. Sixteen specimens were tested under axial compression to study the influence of different CAM thicknesses (the middle height of CAM component), layers of CFRP, and concrete strength on bearing capacity, deformation performance, and stress-strain relationship.

2. Experimental Program

2.1. Test Specimens. All of the specimens were 100 mm × 100 mm in cross section and 300 mm in height. Twelve specimens were C-C-CFSST columns, two specimens were CFRP-confined CFSST columns, and two specimens were CFSST columns. Sixteen specimens were divided into two groups according to the concrete strength. The specimens of group 1 were C20, and those of group 2 were C30. Each group had six C-C-CFSST specimens with 5, 10, and 15 mm CAM thickness. The corresponding radius of rounded corners was 20, 30, and 40 mm. T700 CFRP sheets with 1.72% elongation were used in this test. The performances of steel tubes, epoxy adhesive, and CFRP sheets were tested in a structural laboratory, as shown in Table 1. The test specimens are listed in Table 2. The cross section and FRP bonding position of specimens are shown in Figure 1.

The concrete specimens were prepared with Portland cement. The diameter of the coarse aggregate was 5–10 mm, which was used for fine aggregate in continuous grading and medium sand. The axial compressive strength measured values of two groups' specimens were 20.7 and 27.1 MPa.

The main processes of specimen preparation are as follows: (1) Prefabricated CAM was configured with a high mark cement mortar, and the CAM mold was made with a PVC tube and a plate. The specimen and the CAM should have similar strength values to satisfy the equal-strength principle. The test using CAM strength was slightly higher than the specimen. (2) The epoxy resin was smeared on the surface of the steel tube, and the CAM was bonded on corresponding positions. (3) The CAM components were fixed to dry using adjustable circular steel rings for 48 h. (4) The specimens were wrapped with CFRP sheets after circularizing. The overlap length of the CFRP was 100 mm. The making process of specimen is shown in Figure 2.

2.2. Test Setup and Instrumentation. All specimens were tested under axial compression using a pressure testing machine with 2000 kN capacity. Four axial strain gauges and four hoop strain gauges were pasted on the mid-height of the specimen. Four linear variable differential transducers (LVDTs) were used to monitor the axial deformation of specimens. The LVDTs were installed at the corner of the specimen and covered the mid-height of the specimen. The layout of the test setup and measuring point are shown in Figure 3. The loading program was based on standard for test method of concrete structures (GB/T 50152–2012) [23]. To avoid the premature failure of specimens, the top and bottom ends of specimens were wrapped with additional two layers of CFRP with 50 mm width.

3. Test Results and Discussion

3.1. Main Test Results. The key test results of axial compression specimens are shown in Table 3. f_{c0} is the compressive strength of unconfined concrete columns, f_{co}' is the compressive strength calculated value of CFSST, and N is the ultimate bearing capacity of specimens.

3.2. Test Failure Modes. The typical failure mode of specimens is shown in Figure 4. The tested CFRP-confined CFSST columns failed by CFRP jacket rupture near the corners. These ruptures occurred in the mid-height region of all the specimens. The failure mode of C-C-CFSST columns was similar to CFRP-confined concrete columns.

The specific breakpoint locations of test specimens after loading are shown in Figure 5. L is the horizontal distance from the breakpoint to the corner. The CFRP-confined CFSST column failed by CFRP rupture at the corner of the steel tube because of stress concentration. The CFRP breakpoints of C-C-CFSST columns occurred away from the corner when CAM thickness increases from 5 mm to 15 mm. The changing position of CFRP breakpoints showed that the stress concentration of the steel tube corner gradually reduced with the increasing CAM thickness.

3.3. Load-Strain Response. Figure 6 shows the load-strain curves of C-C-CFSST specimens (group 2). The axial and hoop strains were obtained by the average of four axial strain gauges and four hoop strain gauges, respectively. For specimens C30-5-1-11, C30-10-1-13, and C30-15-1-15, the ultimate load is 738.3, 843.9, and 893.4 kN, respectively. For specimens C30-5-2-12, C30-10-2-4, and C30-15-2-16, the ultimate load is 867.1, 950.3, and 1069.8 kN, respectively. Similar to those FRP-confined concrete load-strain curves, all specimens' curves showed the same trend with a bilinear shape and a monotonically ascending characteristic. When the load was less than 80% of the ultimate load, the axial and hoop strain developed slowly. When the load was more than 80% of the ultimate load, the curves came into the plastic stage, and the deformation grew rapidly. The hoop rupture failure of CFRP occurred when reaching the ultimate loads of specimens, and the ultimate hoop strain slightly increased with the increasing CAM thickness.

Table 1: Material properties.

Materials	Thickness (mm)	Yield strength (MPa)	Tensile strength (MPa)	Tensile elastic modulus (MPa)
Steel tube	2	313.9	392.6	2.07×10^5
CFRP	0.167	—	3094	2.44×10^5
Epoxy resin	—	—	58	2.584×10^3

Table 2: Test parameters of specimens.

Specimen	CAM thickness	Confinement condition
C20-0-0-1	—	—
C20-0-1-2	—	1-layer CFRP confinement
C20-5-1-3	5 mm	1-layer CFRP confinement
C20-5-2-4	5 mm	2-layer CFRP confinement
C20-10-1-5	10 mm	1-layer CFRP confinement
C20-10-2-6	10 mm	2-layer CFRP confinement
C20-15-1-7	15 mm	1-layer CFRP confinement
C20-15-2-8	15 mm	2-layer CFRP confinement
C30-0-0-9	—	—
C30-0-1-10	—	1-layer CFRP confinement
C30-5-1-11	5 mm	1-layer CFRP confinement
C30-5-2-12	5 mm	2-layer CFRP confinement
C30-10-1-13	10 mm	1-layer CFRP confinement
C30-10-2-14	10 mm	2-layer CFRP confinement
C30-15-1-15	15 mm	1-layer CFRP confinement
C30-15-2-16	15 mm	2-layer CFRP confinement

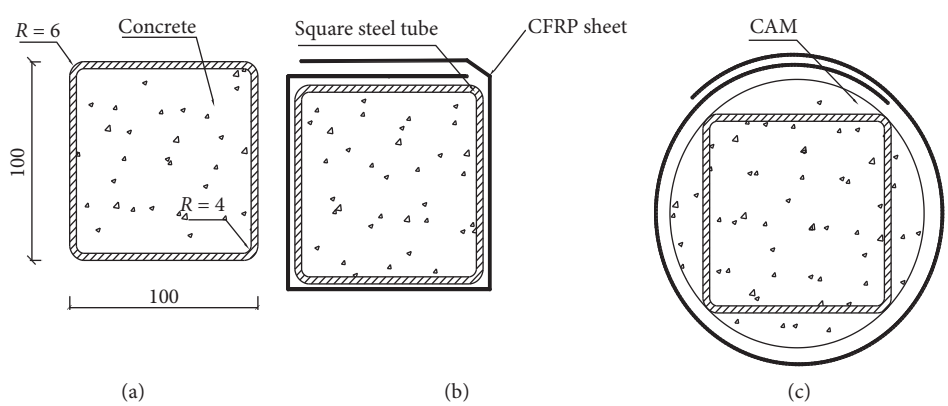

Figure 1: Cross sections of specimens. (a) CFSST column. (b) CFRP-confined CFSST column. (c) C-C-CFSST column.

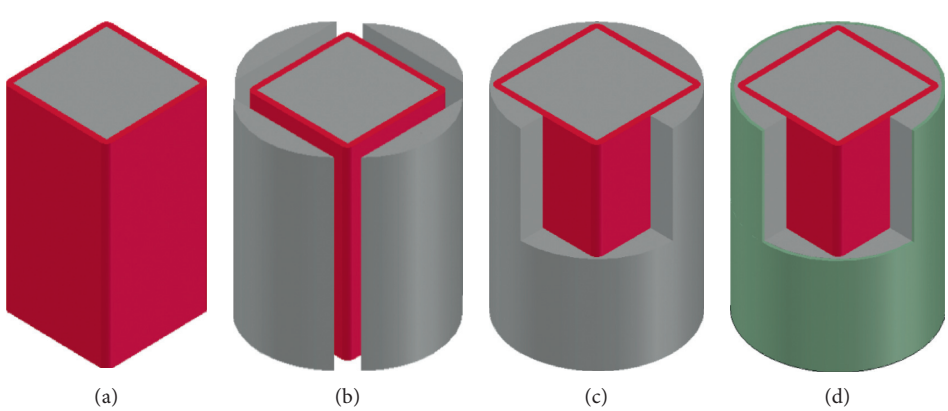

Figure 2: Production process of specimens. (a) CFSST column. (b) CAM bonding. (c) CAM fixing. (d) CFRP wrapping.

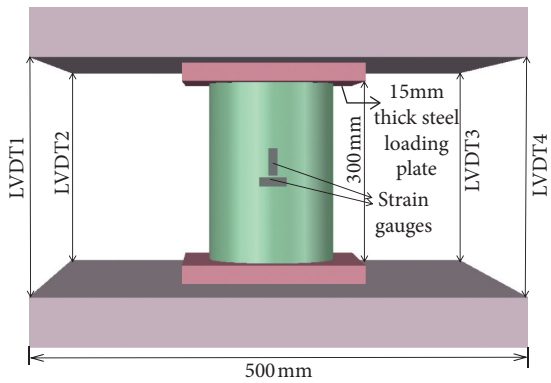

Figure 3: Loading apparatus and LVDTs.

Table 3: Experimental results of specimens.

Specimen	f_{c0} (MPa)	f_{co}' (MPa)	N (kN)
C20-0-0-1	20.7	45.82	488.0
C20-0-1-2	20.7	45.82	542.7
C20-5-1-3	20.7	45.82	650.5
C20-5-2-4	20.7	45.82	765.0
C20-10-1-5	20.7	45.82	760.0
C20-10-2-6	20.7	45.82	875.6
C20-15-1-7	20.7	45.82	800.4
C20-15-2-8	20.7	45.82	1019.3
C30-0-0-9	27.1	53.39	539.9
C30-0-1-10	27.1	53.39	631.6
C30-5-1-11	27.1	53.39	738.3
C30-5-2-12	27.1	53.39	867.1
C30-10-1-13	27.1	53.39	843.9
C30-10-2-14	27.1	53.39	950.3
C30-15-1-15	27.1	53.39	893.4
C30-15-2-16	27.1	53.39	1069.8

3.4. CAM Influence on Bearing Capacity and Vertical Displacement. Figures 7 and 8 show vertical displacement and bearing capacity of test specimens with different CAM thickness. When the CAM thickness increases from 5 mm to 15 mm, the bearing capacity and vertical displacement increase gradually. Compared with C20-0-1-2, the bearing capacity of C20-5-1-3, C20-10-1-5, and C20-15-1-7 increased by 19.9%, 40.2%, and 47.5%, respectively. Compared with C30-0-1-10, the bearing capacity of C30-5-1-11, C30-10-1-13, and C30-15-1-15 increased by 16.9%, 33.6%, and 41.4%, respectively. The increasing bearing capacity and vertical displacement showed the great effectiveness of CAM between CFRP sheets and CFSST columns. The increase of the CAM thickness generally leads to an increase in the bearing capacity and vertical displacement, which indicated that the circularization technique for strengthening CFSST short columns is a suitable and alternative strengthening method in engineering.

4. Stress-Strain Models of CFSST Columns

4.1. Axial Stress-Strain Curves. The axial stress-axial strain curves of all the test specimens are shown in Figure 9. All the curves had an obvious bilinear shape with two segments. The first-segment slope of the curve was much bigger than the second-segment slope. The CAM thickness affected mainly the second segment of the stress-strain curve. The second-segment slopes of C-C-CFSST specimens became slightly larger with the increase of CAM thickness. The ultimate axial stress f_{cc}' was affected by the CAM thickness and the layers of CFRP. As for specimens with no CAM, f_{cc}' and the second-segment slope were the smallest. The stress-strain curve of C20-5-1-3 and C30-5-1-11 was close to the stress-strain curve of C20-0-1-2 and C30-0-1-11, respectively, showing that CFRP wrapping was less effective for specimens with a CAM thickness of 5 mm. The specimens with a CAM thickness of 10 or 15 mm increased the effectiveness of CFRP confinement. To ensure the strengthening effectiveness in practical engineering, the CAM thickness should be large. The layers of CFRP affected f_{cc}' and ductility. The ultimate axial strain $\varepsilon_{cc}'$and ultimate axial stress f_{cc}' of specimens with two layers of CFRP were significantly larger than those of specimens with one layer of CFRP.

4.2. Existing Stress-Strain Models. The existing FRP-confined concrete stress-strain models are mainly separated into two types. The first type uses a single function to express the stress-strain relationship and includes the Mander model, Samaan model, Yu model, and Yang and Feng model [24–27]. The second type uses piecewise function to express the stress-strain relationship and includes the Lam and Teng model, Lai model, Miyauchi model, and Wei and Wu model [28–34]. Among all existing models, the Lam and Teng model, Lai model, and Yang model are appropriate to predict the stress-strain relationship of CFRP-confined circularized concrete columns according to the published literature [8, 27].

4.2.1. Lam and Teng Model. The first segment of the Lam and Teng model is a parabolic type, and the second segment is a linear type. This model has a high degree of accuracy in predicting FRP-confined concrete strength. The model is described by the following equation:

$$\begin{cases} \sigma_c = E_c\varepsilon_c - \dfrac{(E_c - E_2)}{4f_0}\varepsilon_c^2 \left(0 \le \varepsilon_c \le \varepsilon\right)_t, \\ \sigma_c = f_{co}' + E_2\varepsilon_c \left(\varepsilon_t \le \varepsilon_c \le \varepsilon_{cu}\right), \end{cases} \tag{1}$$

where σ_c and ε_c are the axial stress and axial strain, respectively. The ultimate axial stress and the ultimate strain are calculated as follows:

$$\begin{aligned} \frac{f_{cc}'}{f_{co}'} &= 1 + 3.3k_1\frac{f_l}{f_{co}'}, \\ \frac{\varepsilon_{cu}}{\varepsilon_{co}} &= 1.75 + 12k_s\frac{f_l}{f_{co}}\left(\frac{\varepsilon_{ru}}{\varepsilon_{co}}\right)^{0.45}, \end{aligned} \tag{2}$$

where ε_{ru} is the confinement effectiveness coefficient k_1 and transition strain ε_t is given as follows:

Figure 4: Failure mode of some specimens.

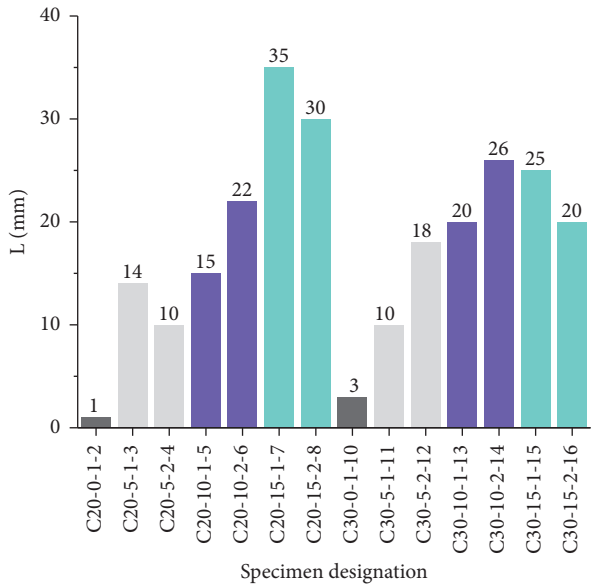

Figure 5: Influence of CAM thickness on CFRP breakpoint location.

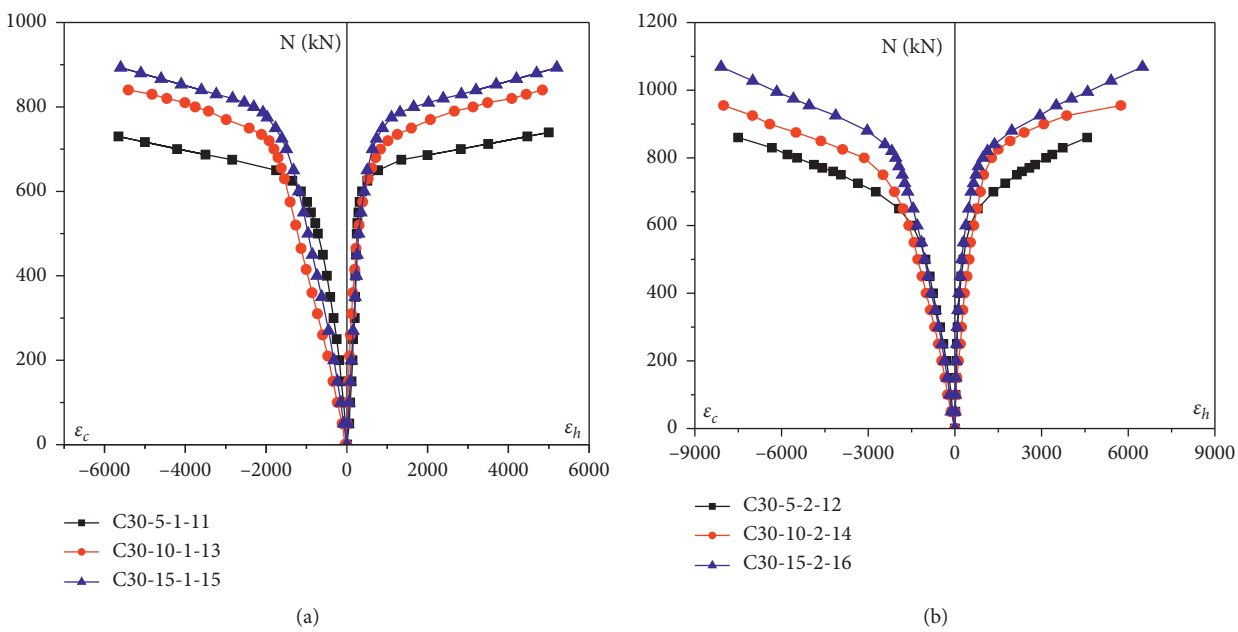

Figure 6: Test load-strain curves. (a) Specimens warped with one-layer CFRP. (b) Specimens warped with two-layer CFRP.

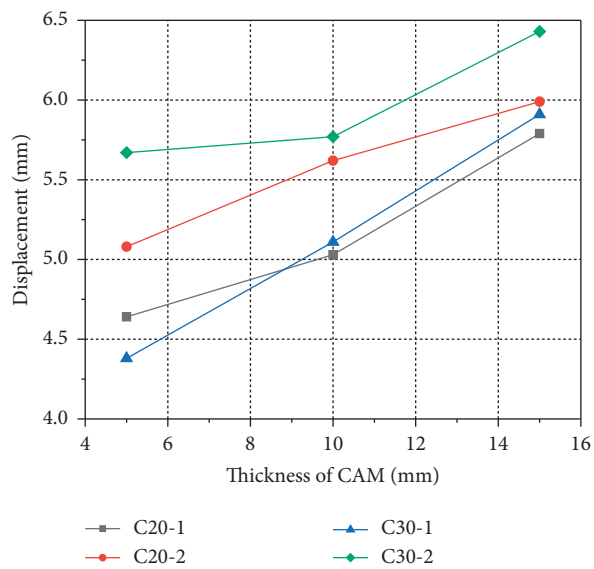

Figure 7: The effects of CAM thickness on vertical displacement.

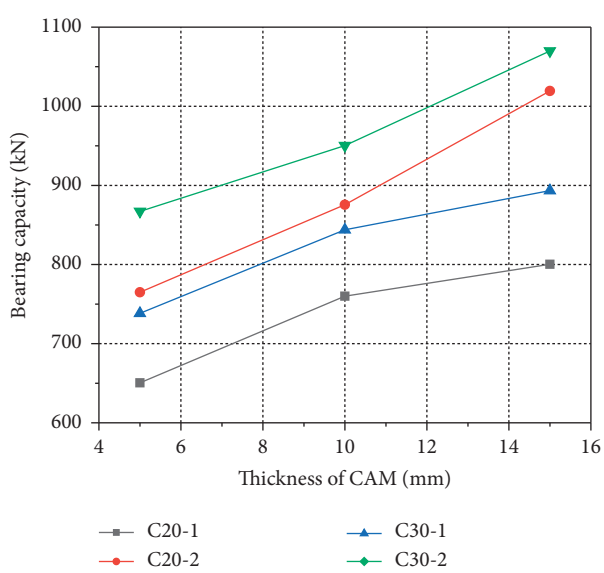

Figure 8: The effects of CAM thickness on bearing capacity.

$$k_s = 1 - \frac{(b-2r)^2 + (h-2r)^2}{3A_{\text{cor}}},$$
$$\varepsilon_t = \frac{2f_0}{E_c - E_2}, \tag{3}$$

where $E_c = 4730\sqrt{f'_{co}}$ is the elastic modulus of the unconfined concrete, $E_2 = (f'_{cc} - f_0)/\varepsilon_{cu}$ is the slope of the linear second portion, $\varepsilon_{co} = 0.002$ is the axial strain with ultimate load, and k_s is the constraint coefficient.

4.2.2. Lai Model. The Lai model has a high accuracy to predict the CFRP-confined rectangular concrete column with corner radii, which is described by the following equation:

$$\begin{cases} \sigma_z = \dfrac{\varepsilon_z}{A + B\varepsilon_z + C\varepsilon_z^2}, & 0 \le \varepsilon_z \le \varepsilon_{zb}, \\ \sigma_z = \sigma_{zb} + E_2(\varepsilon_z - \varepsilon_{zb}), & \varepsilon_{zb} \le \varepsilon_z \le \varepsilon_{zc}. \end{cases} \tag{4}$$

A, B, and C are given as follows:

$$\begin{cases} A = \dfrac{1}{E_0}, \\ B = \left(\dfrac{1}{E_p} - \dfrac{2}{E_0} + \dfrac{1}{E_p}\dfrac{E_2}{E_p}\right), \\ C = \left(\dfrac{1}{E_0} - \dfrac{1}{E_p}\dfrac{E_2}{E_p}\right)\dfrac{1}{\varepsilon_t^2}, \end{cases} \tag{5}$$

where $E_p = \sigma_{zb}/\varepsilon_{zb}$.

FRP-confined concrete E_2/E_c in different sections is given as follows:

$$\frac{E_2}{E_c} = \begin{cases} 0.0331\ \ln(\beta_j) - 0.0564, & \beta_j \ge 5.6, \\ 0.1217\ \ln(\beta_j) - 0.2091, & \beta_j < 5.6. \end{cases} \tag{6}$$

Constraint stiffness β_j is given as follows:

$$\beta_j = \frac{E_f t_f}{f_c R}, \tag{7}$$

where R represents the radii of equivalent circle $= 2(b+h)/2\pi$.

Transition stress and strain are given as follows:

$$\frac{\sigma_{zb}}{f_{c,m}} = 0.0568\beta_j^{0.46} + 1,$$
$$\frac{\varepsilon_t}{\varepsilon_{cu}} = 0.011\beta_j + 1. \tag{8}$$

4.2.3. Yang and Feng Model. The Yang and Feng model is different from the two above models, which have no obvious transition segment. This model has high accuracy to predict the CFRP-confined concrete column, which is given as follows:

$$\sigma_c = \frac{(\varepsilon_c/\varepsilon_{cc}^*) f_{cc}^* r}{r - 1 + (\varepsilon_c/\varepsilon_{cc}^*) r},$$
$$r = \frac{E_c}{E_c - (f_{cc}^*/\varepsilon_{cc})},$$
$$\frac{f_{cc}^*}{\varepsilon_{cc}} = 1 + 3.33\left(\frac{\sigma_l}{f'_{co}}\right)^{0.9}, \tag{9}$$
$$\frac{\varepsilon_{cc}^*}{\varepsilon_{cc}} = 1 + 17.4\left(\frac{\sigma_l}{f'_{co}}\right)^{1.07}.$$

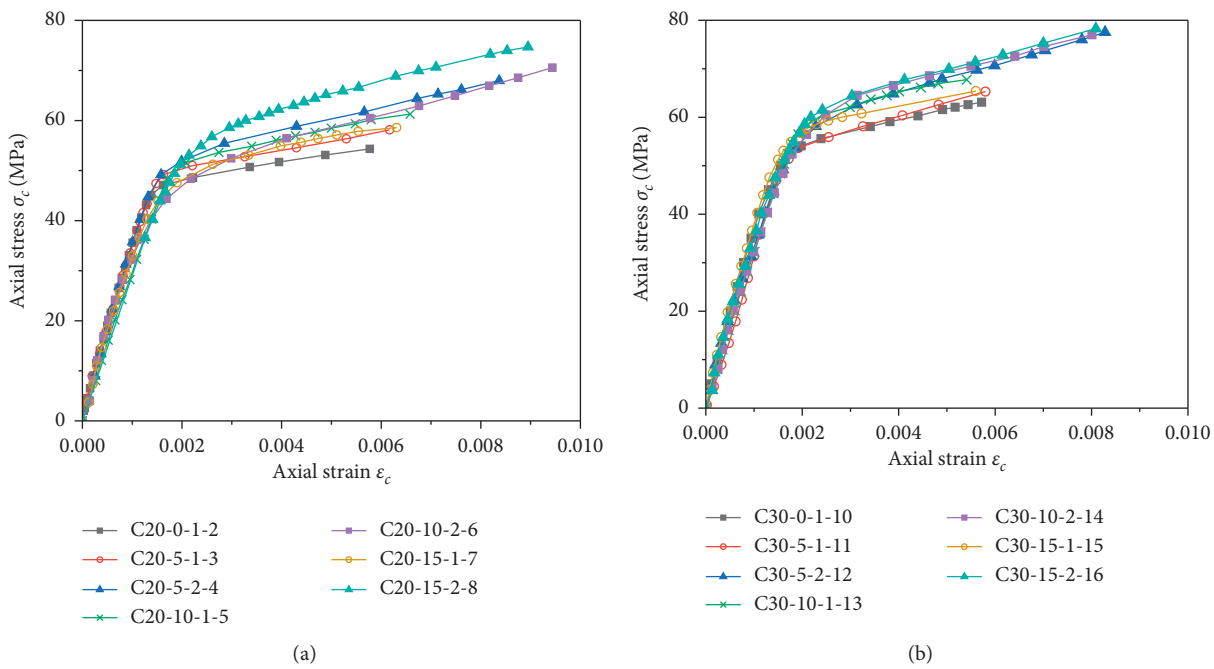

Figure 9: Test stress-strain curves. (a) Specimens of group C20. (b) Specimens of group C30.

where f_{cc}^* and ε_{cc}^* are the peak axial stress and corresponding axial strain of concrete under a specific level of lateral confining stress.

4.3. CFSST Column Strength f'_{co}. CFSST column strength f'_{co} is given in *technical code for concrete filled steel tubular structures* (GB50936-2014) [35]. It is calculated as follows:

$$f'_{co} = \left(1.212 + B\theta_{sc} + C\theta_{sc}^2\right) f_{co},$$
$$B = \frac{0.131 f_y}{235} + 0.723,$$
$$C = -\left(\frac{0.07 f_{ck}}{14.4}\right) + 0.026, \quad (10)$$
$$\theta_{sc} = \alpha_{sc}\frac{f}{f_c},$$
$$\alpha_{sc} = \frac{A_s}{A_c},$$

where A_s and A_c are the steel tube area and core concrete area, respectively; f_y and f are the tensile strength standard value and design value, respectively; α_{sc} and θ_{sc} are the steel ratio and confinement coefficient of the specimen, respectively; B and C are the influence coefficients.

4.4. Effective CFRP Confinement Coefficient k_e. The theoretical fracture strain ε_{fu} can be calculated as fiber strength divided by the elastic modulus. However, the actual fracture strain ε_{ru} is much smaller than the theoretical fracture strain. Lam and Teng suggested that ε_{ru} can be calculated from ε_{fu} as follows:

$$\varepsilon_{ru} = k_e \varepsilon_{fu}, \quad (11)$$

where the effective CFRP confinement coefficient k of the circular column is approximately 0.586 [15] and was taken as 0.5, 0.53, and 0.56 corresponding with CAM thickness of 5, 10, and 15 mm, respectively, according to the test results.

4.5. Intercept of the Stress Axis by the Linear Second Portion f_0. Lam and Teng showed $f_0/f'_{co} = 1.09$ from the test and suggested that $f_0 = f'_{co}$ approximately [15]. However, this method ignores the influence of FRP confinement. The intercept f_0 was affected by the confinement effectiveness, which can be calculated by confinement stiffness ratio β_j and confining factor ξ. Yu [26] suggested that f_0 can be calculated as follows:

$$f_0 = (1 + 1.1\xi) f'_c. \quad (12)$$

However, for FRP-confined CFSST columns, confining factor ξ should value FRP and steel tube confining factor, and f_0 is given as follows:

$$\frac{f_0}{f'_{co}} = 1 + k\xi, \quad (13)$$

where k is modified based on the test results. The linear fitting between f_0/f'_{co} and ξ is shown in Figure 10, and $k = 0.04854$.

4.6. Stress-Strain Model Verification. The experimental stress-strain curves of 12 C-C-CFSST columns were compared with the calculation curves of the Lam and Teng

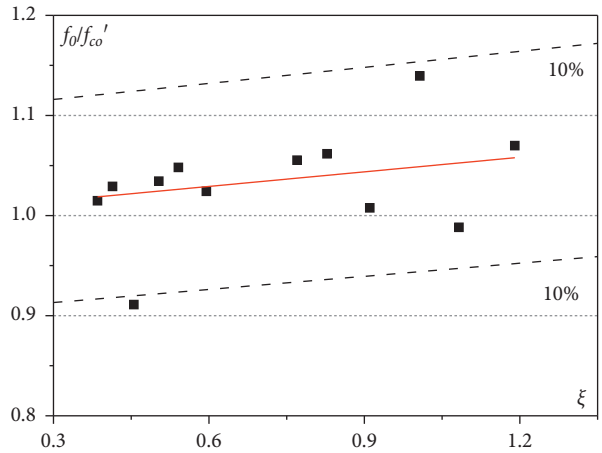

Figure 10: Relationship between f_0/f_{co}' and ξ.

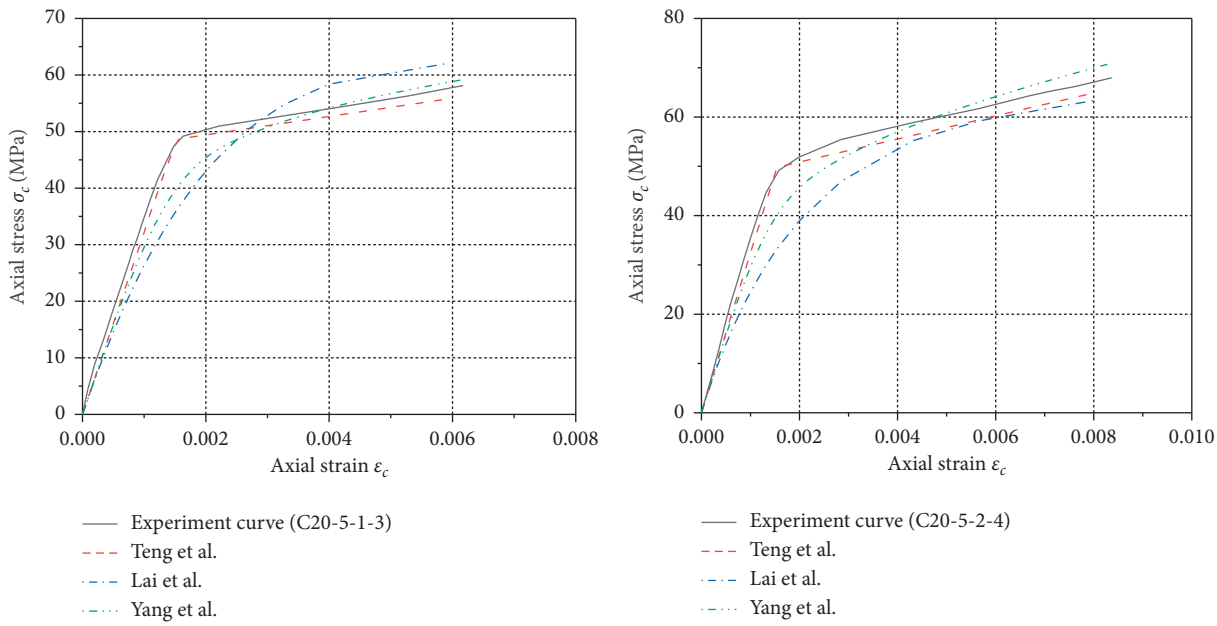

(a) (b)

Figure 11: Continued.

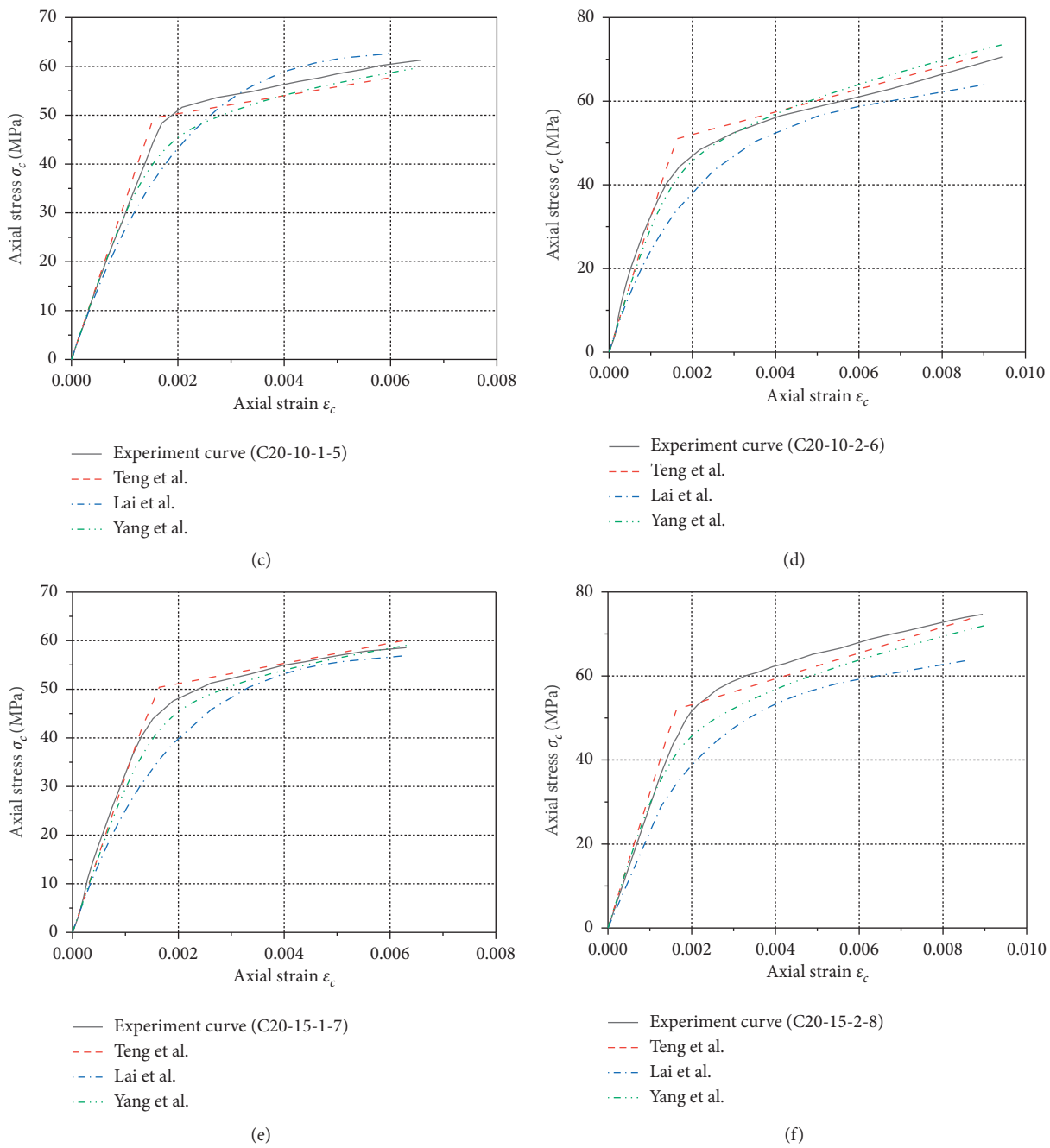

Figure 11: Comparison of calculated stress-strain curves with the experiment curve of group C20. (a) C20-5-1-3. (b) C20-5-2-4. (c) C20-10-1-5. (d) C20-10-2-6. (e) C20-15-1-7. (f) C20-15-2-8.

model, Lai model, and Yang and Feng model. The comparison of calculated stress-strain curves with experiment curve is shown in Figures 11 and 12.

The Lam and Teng model had the highest fitting grade on C-C-CFSST column stress-strain curves among three models. The Yang and Feng model fitted well in some situations, such as C20-10-2-6, C20-15-1-7, C30-5-1-11, and C30-15-2-16. The Lai model had a big deviation compared with other models. The stress-strain curves of the C-C-CFSST column can be separated into three segments, as shown in Figure 13.

In segment I, the Lam and Teng model shows a great prediction on the stress-strain relationship of the C-C-CFSST column. The Lai model and the Yang and Feng model generally underestimated the axial stress of specimens in segment I. The Lam and Teng model has an unobvious segment II slightly overestimating the axial stress. The Yang and Feng model has a similar trend to the experiential curves of segment II. Although similar to segment I, this model underestimates the axial stress of specimens. The Lai model also greatly underestimates the axial stress because of the inaccuracy of the calculated transition strain. In segment III, the ultimate axial stress f'_{cc} calculated

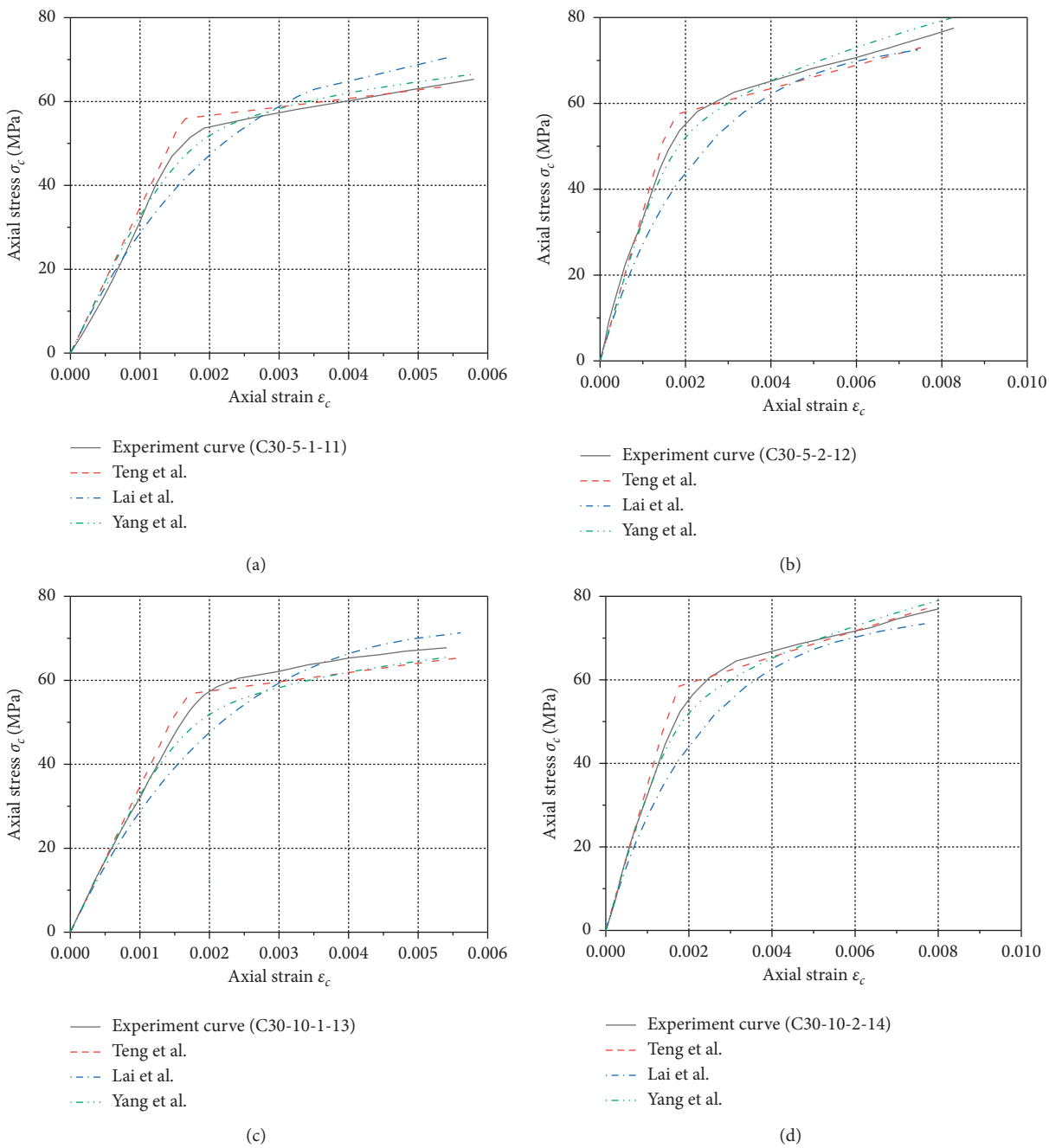

Figure 12: Continued.

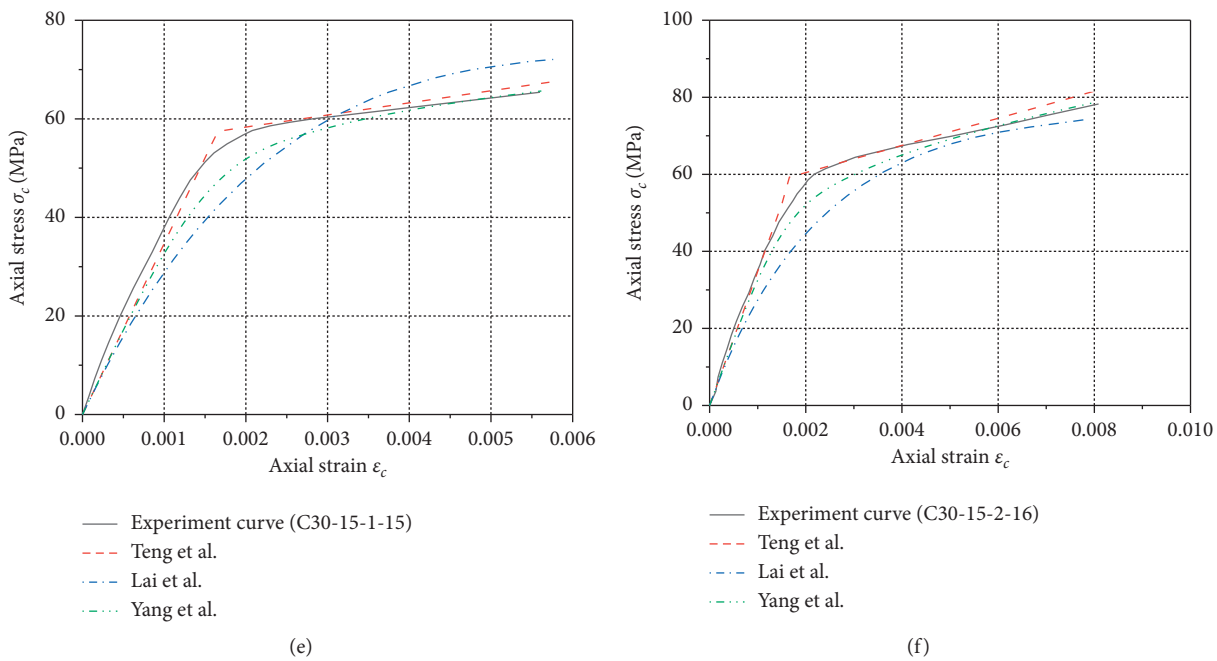

Figure 12: Comparison of calculated stress-strain curves with the experiment curve of group C30. (a) C30-5-1-11. (b) C30-5-2-12. (c) C30-10-1-13. (d) C30-10-2-14. (e) C30-15-1-15. (f) C30-15-2–16.

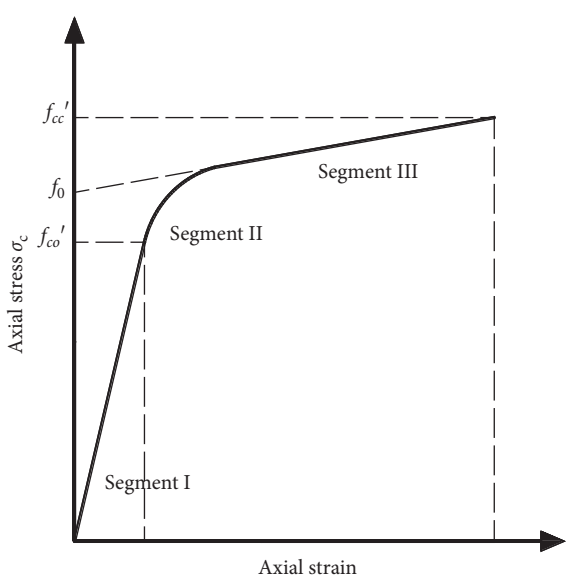

Figure 13: Proposed stress-strain model for C-C-CFSST.

from the Lam and Teng model and the Yang and Feng model is well estimated to the test value. The stress-strain curves calculated from the Lam and Teng model are dramatically close to the test curves. In conclusion, the Lam and Teng model has the greatest prediction for the stress-strain relationship of the C-C-CFSST column among the three models. The Yang model has a more accurate prediction, while CAM thickness is increasing. The transition strain of the Lai model is always larger than the test transition strain, which leads to the inaccuracy of the calculated curves. A more accurate stress-strain model for C-C-CFSST columns should be developed in experimental and theoretical research.

5. Conclusions

This study presents the results from an experimental investigation on the compressive behavior of 16 C-C-CFSST short columns. Based on test data, the effect of CAM thickness on the failure model and the axial stress-strain relationship is discussed. The following conclusions can be made:

(1) CFRP confinement using the CAM could effectively enhance the ductility and axial load carrying capacity of CFSST short columns. For the increasing CAM thickness, the bearing capacity of C20-5-1-3, C20-10-1-5, and C20-15-1-7 is improved by 19.9%, 40.2%, and 47.5%, respectively.

(2) The increasing CAM thickness leads to the CFRP breakpoint gradually moving far from the specimen corner, which led to the decrease of stress concentration of CFRP hoop stress in the corner of the square steel tube. The increasing CAM thickness also made the lateral stress well distributed. The effective fracture strain and constraint efficiency of CFRP increased well.

(3) The stress-strain curve characteristic of the C-C-CFSST column is similar to the CFRP-confined circular concrete column. The applicability of the existing model for FRP-confined concrete was evaluated and compared with the test data. The predictions of the Lam and Teng model agree well with the test data.

Data Availability

The data used to support the findings of this study are listed in this paper.

Conflicts of Interest

The authors declare no conflicts of interest regarding the publication of this paper.

Acknowledgments

This research work was financially supported by the National Natural Science Foundation of China (Grant no. 42072296).

References

[1] X. Zhou, D. Gan, J. Liu, and S. Zhang, "Experiment and analysis on square tubed reinforced concrete stub columns under axial compression," *Journal of Building Structures*, vol. 32, no. 1, pp. 68–74, 2011.

[2] J. Wang, Q. Shen, F. Wang, and W. Wang, "Experimental and analytical studies on CFRP strengthened circular thin-walled CFST stub columns under eccentric compression," *Thin-Walled Structures*, vol. 127, pp. 102–119, 2018.

[3] Y.-X. Hua, L.-H. Han, Q.-L. Wang, and C. Hou, "Behaviour of square CFST beam-columns under combined sustained load and corrosion: experiments," *Thin-Walled Structures*, vol. 136, pp. 353–366, 2019.

[4] C. Hou, L.-H. Han, and X.-L. Zhao, "Full-range analysis on square CFST stub columns and beams under loading and chloride corrosion," *Thin-Walled Structures*, vol. 68, pp. 50–64, 2013.

[5] F. Zhang, J. Xia, G. Li et al., "Degradation of axial ultimate load-bearing capacity of circular thin-walled concrete-filled steel tubular stub columns after corrosion," *Materials*, vol. 13, no. 3, 2020.

[6] H. Huang, Y. Xu, L. Guo et al., "Axial compressive behavior of CFRP-reinforced circular concrete-filled steel tubular stub columns with local corrosion," *Journal of Building Structures*, vol. 41, pp. 109–116, 2020.

[7] S. Zhong, "Application and development in China of concrete filled steel tubular structure," *Architecture Technology*, vol. 02, pp. 80–82, 2001.

[8] J. Zhu, G. Lin, J. Teng et al., "FRP-confined square concrete columns with section curvilinearization under axial compression," *Journal of Composites for Construction*, vol. 24, no. 2, 2020.

[9] Y. Wang, G. Chen, B. Wan et al., "Behavior of circular ice-filled self-luminous FRP tubular stub columns under axial compression," *Construction and Building Materials*, vol. 232, 2020.

[10] Y. Guo and Y. Zhang, "Comparative study of CFRP-confined CFST stub columns under axial compression," *Advances in Civil Engineering*, vol. 18, Article ID 7109061, 8 pages, 2018.

[11] H. Elsanadedy, T. Almusallam, Y. Al-Salloum, and R. Iqbal, "Effect of high temperature on structural response of reinforced concrete circular columns strengthened with fiber reinforced polymer composites," *Journal of Composite Materials*, vol. 51, no. 3, pp. 333–355, 2017.

[12] J. Liang, W. Zou, Z. Wang, and D. Liu, "Compressive behavior of CFRP-confined partially encased concrete columns under axial loading," *Composite Structures*, vol. 229, 2019.

[13] X. Song, X. Gu, Y. Li, T. Chen, and W. Zhang, "Mechanical behavior of FRP-strengthened concrete columns subjected to concentric and eccentric compression loading," *Journal of Composites for Construction*, vol. 17, no. 3, pp. 336–346, 2013.

[14] T. Zhong, "State of the art of concrete filled square steel columns," *Building Structure*, vol. 7, pp. 20–23, 2003.

[15] Z. Tao and L.-H. Han, "Behaviour of fire-exposed concrete-filled steel tubular beam columns repaired with CFRP wraps," *Thin-Walled Structures*, vol. 45, no. 1, pp. 63–76, 2007.

[16] J. Dong, Q. Wang, and Z. Guan, "Structural behaviour of recycled aggregate concrete filled steel tube columns strengthened by CFRP," *Engineering Structures*, vol. 48, pp. 532–542, 2013.

[17] Z. Tao, L.-H. Han, and J.-P. Zhuang, "Axial loading behavior of CFRP strengthened concrete-filled steel tubular stub columns," *Advances in Structural Engineering*, vol. 10, no. 1, pp. 37–46, 2007.

[18] Q. Wang, Y. Xue, Y. Shao, and X. Yan, "Study of static performance of axially compressed concrete filled square steel tubular stub columns confined by CFRP," *China Civil Engineering Journal*, vol. 41, pp. 32–39, 2011.

[19] F. Seible and M. J. N. Priestley, "Strengthening of rectangular bridge columns for increased ductility," in *Proceeding of the Symposium on Practical Solutions for Bridge Strengthening & Rehabilitation*, pp. 239–248, Des Moines, IA, USA, April 1993.

[20] M. N. S. Hadi, T. M. Pham, and X. Lei, "New method of strengthening reinforced concrete square columns by circularizing and wrapping with fiber-reinforced polymer or steel straps," *Journal of Composites for Construction*, vol. 17, no. 2, pp. 229–238, 2013.

[21] M. T. Jameel, M. N. Sheikh, and M. N. S. Hadi, "Behaviour of circularized and FRP wrapped hollow concrete specimens under axial compressive load," *Composite Structures*, vol. 171, pp. 538–548, 2017.

[22] W. Yang, Y. Zhang, J. Chai, G. Wu, and Z. Dong, "Experimental investigation of rectangular concrete-filled fiber reinforced polymer (FRP)-steel composite tube columns for various corner radii," *Composite Structures*, vol. 244, 2020.

[23] National Standard of the People's Republic of China, *Standard For test Method of Concrete Structures. GB/T 50152-2012*, China Architecture & Building Press, Beijing, China, 2012.

[24] J. B. Mander, M. J. N. Priestley, and R. Park, "Theoretical stress-strain model for confined concrete," *Journal of Structural Engineering*, vol. 114, no. 8, pp. 1804–1826, 1988.

[25] M. Samaan, A. Mirmiran, and M. Shahawy, "Model of concrete confined by fiber composites," *Journal of Structural Engineering*, vol. 124, no. 9, pp. 1025–1031, 1998.

[26] Q. Yu, "Stress-strain relationship of FRP-confined concrete subjected to axial compression," *Industrial Construction*, vol. 4, pp. 5–8, 2001.

[27] L. Lam and J. Teng, "Design-oriented stress–strain model for FRP-confined concrete," *Construction & Building Materials*, vol. 17, no. 6-7, pp. 471–489, 2003.

[28] J. G. Teng, T. Jiang, L. Lam, and Y. Z. Luo, "Refinement of a design-oriented stress-strain model for FRP-confined concrete," *Journal of Composites for Construction*, vol. 13, no. 4, pp. 269–278, 2009.

[29] J. Yang and P. Feng, "Analysis-oriented models for FRP-confined concrete: 3D interpretation and general methodology," *Engineering Structures*, vol. 219, 2020.

[30] W. Lai, J. Pan, and X. Jin, "Compressive stress-strain behavior of concrete confined by fiber reinforced polymer," *Industrial Construction*, vol. 10, pp. 81–84, 2004.

[31] X. Jin, J. Pan, G. Liu, and W. Lai, "Research of stress-strain curve of concrete confined by fiber reinforced plastics under

axial compression," *Journal of Building Structures*, vol. 04, pp. 47–53, 2003.

[32] J. Pan, Y. Wang, and W. Lai, "Effect of sectional shape of concrete column on the bearing capacity of short columns wrapped with FRP," *Industrial Construction*, vol. 06, pp. 17–19, 2001.

[33] K. Miyauchi, S. Inoue, T. Kuroda et al., "Strengthening effects of concrete column with carbon fiber sheet," *Transactions of the Japan Concrete Institute*, vol. 21, pp. 143–150, 1999.

[34] Y.-Y. Wei and Y.-F. Wu, "Unified stress-strain model of concrete for FRP-confined columns," *Construction and Building Materials*, vol. 26, no. 1, pp. 381–392, 2012.

[35] National Standard of the People's Republic of China, *Technical Code for Concrete Filled Steel Tubular Structures. GB 50936-2014*, China Architecture & Building Press, Beijing, China, 2014.